Determination of the ReA Electron Beam Ion Trap electron beam radius and current density with an X-ray pinhole camera

Thomas M. Baumann, Alain Lapierre, Kritsada Kittimanapun, Stefan Schwarz, Daniela Leitner, and Georg Bollen

Citation: Review of Scientific Instruments **85**, 073302 (2014); doi: 10.1063/1.4885448
View online: https://doi.org/10.1063/1.4885448
View Table of Contents: http://aip.scitation.org/toc/rsi/85/7
Published by the American Institute of Physics

Determination of the ReA Electron Beam Ion Trap electron beam radius and current density with an X-ray pinhole camera

Thomas M. Baumann,[a] Alain Lapierre,[b] Kritsada Kittimanapun, Stefan Schwarz, Daniela Leitner, and Georg Bollen

National Superconducting Cyclotron Laboratory (NSCL), Michigan State University (MSU), 640 S. Shaw Lane, East Lansing, Michigan, 48824, USA

(Received 30 May 2014; accepted 14 June 2014; published online 3 July 2014)

The Electron Beam Ion Trap (EBIT) of the National Superconducting Cyclotron Laboratory at Michigan State University is used as a charge booster and injector for the currently commissioned rare isotope re-accelerator facility ReA. This EBIT charge breeder is equipped with a unique superconducting magnet configuration, a combination of a solenoid and a pair of Helmholtz coils, allowing for a direct observation of the ion cloud while maintaining the advantages of a long ion trapping region. The current density of its electron beam is a key factor for efficient capture and fast charge breeding of continuously injected, short-lived isotope beams. It depends on the radius of the magnetically compressed electron beam. This radius is measured by imaging the highly charged ion cloud trapped within the electron beam with a pinhole camera, which is sensitive to X-rays emitted by the ions with photon energies between 2 keV and 10 keV. The 80%-radius of a cylindrical 800 mA electron beam with an energy of 15 keV is determined to be $r_{80\%} = (212 \pm 19)\mu$m in a 4 T magnetic field. From this, a current density of $j = (454 \pm 83)$A/cm^2 is derived. These results are in good agreement with electron beam trajectory simulations performed with TriComp and serve as a test for future electron gun design developments. © *2014 AIP Publishing LLC*. [http://dx.doi.org/10.1063/1.4885448]

I. INTRODUCTION

The rare isotope re-accelerator ReA at the National Superconducting Cyclotron Laboratory (NSCL) at Michigan State University (MSU) has been brought into operation recently.[1] It accelerates low-energy beams obtained from gas stopping[2] of high-energy fragments to energies of up to several MeV/u. ReA employs a novel Electron Beam Ion Trap (EBIT) charge breeder[3] as an injector for a room-temperature radio-frequency quadrupole accelerator prior to further acceleration in a superconducting linear accelerator.

Pulsed injection is an established technique for efficient capture of ions into electron beam ion traps or sources. The disadvantage of this method, however, is the need for a "buncher" ion trap[4] to accumulate continuous beams and produce pulses, which adds complexity to the entire re-acceleration system. Furthermore, such a trap can be affected by large losses due to its limited space charge capacity,[5] which is especially problematic for high ion beam currents as expected for the future FRIB facility.[6] To overcome this constraint, the ReA-EBIT is designed for continuous ion injection into a high current electron beam, where the ions are accumulated and charge bred simultaneously. The capture efficiency of this injection mode strongly depends on the electron beam current density, which is also of importance for fast charge breeding of short-lived isotopes. To reach a sufficient current density, the ReA-EBIT uses a Pierce-type electron gun design with its cathode partially immersed in the EBIT magnetic fringe field.[7] Unlike the Brillouin-flow mode, this semi-immersed flow mode provides a smaller electron beam compression, but ensures an efficient transport of a high current with losses estimated to be less than 0.1% and produces a more stable beam with a rather invariable radius.[8]

This article presents a measurement of the electron beam radius and current density of the new ReA-EBIT to characterize its performance as a charge breeder. The method chosen for this measurement is to image the electron beam using a pinhole camera sensitive in the X-ray regime. Unlike other existing breeders, this is possible due to the unique magnet configuration of the ReA-EBIT. This technique was first established by Knapp *et al.*[9] on the LLNL EBIT and has been used successfully at different EBIT facilities[10–13] since then. It utilizes X-rays emitted from atomic transitions of trapped highly charged ions after excitation by the electron beam. The advantage of using X-ray emissions is the short lifetime of the involved atomic energy levels (<ns) that lead to a direct imaging of the interaction region of the electron beam with the ion cloud, since the exited ions do not have time to exit the beam before de-excitation and photon emission. In contrast, measurements in the visible regime can reveal an expansion of the ion cloud outside the electron beam by observing photons emitted from metastable states. Such measurements are used to study behavior and thermal properties of the ions for different trapping conditions.[14–16]

After a brief description of the EBIT operation principle and the set-up of the pinhole camera, the measurement and detailed data analysis are discussed. A model is presented to describe the electron-ion overlap, which is needed for extracting the electron beam radius from the data and to determine the current density.

[a]baumannt@nscl.msu.edu
[b]lapierre@nscl.msu.edu

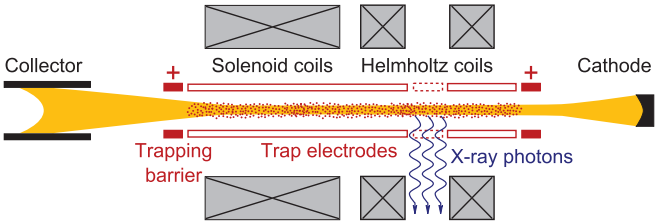

FIG. 1. Schematic view of the ReA-EBIT (not to scale). The ions are trapped by a positive potential applied to the trapping barrier electrodes (marked with "+") in axial direction, while the negative space charge of the electron beam provides a radial trapping potential. X-ray emissions can be observed through the view ports located between the Helmholtz coils. The trap electrode in this region (dashed line) is built with eight radial slits to allow for observation of trapped highly charged ions.

II. ReA-EBIT AND X-RAY PINHOLE CAMERA

The ReA-EBIT[17] uses a magnetically compressed electron beam for producing and trapping highly charged ions (illustrated in Fig. 1). The electron beam is produced from a 6.35-mm diameter Ba-dispenser cathode and injected into a high magnetic field region, where it is compressed to a size of a few hundred micrometers. A series of cylindrical electrodes provide an electrostatic potential well that, together with the negative electron beam space charge, traps the ions. Highly charged ions are produced by successive electron impact ionization. One of the unique features of the ReA-EBIT is the configuration of its superconducting magnet, which consists of a solenoid coil and a pair of Helmholtz coils. This combines the EBIS-like advantages of a long trapping region with the possibility of direct optical access to the ion cloud through the gap between the Helmholtz coils.

In the experiment presented here, the electron beam is imaged using an X-ray pinhole camera. The camera is installed at one of seven accessible radial ports around the gap between the Helmholtz coils. The set-up consists of a stainless steel tube as a vacuum chamber for the CCD camera and an in-air pinhole mounted on an xyz-manipulator (see Fig. 2). The camera vacuum and EBIT vacuum are separated by two Be-windows, which are 127 μm thick each. The air gap between the two windows is about 100 mm. A pressure below 5 $\times$ 10^{-9} Torr is maintained in the EBIT. The camera chamber is kept at a pressure of about 1$\times$ 10^{-2} Torr to minimize the absorption of X-rays along their path. The use of an air gap allows for a simple and accessible pinhole mount.

Since the ion cloud within the electron beam is an X-ray line source, an image obtained by projection on a plane parallel to the propagation direction of the electron beam is sufficient to determine its radius. Thus, a slit oriented along the electron beam is preferable to a pinhole as it allows for a higher photon flux to the CCD detector. The slit assembly provides a fixed slit length of 12.7 mm and an adjustable slit width from 12 mm to 25 μm. The distance between the slit assembly and the CCD is (606 $\pm$ 2) mm, while the slit is placed at a distance of (417 $\pm$ 2)mm from the electron beam. The ratio of those two distances defines the magnification factor of the system of $c_M = (1.45 \pm 0.01)$.

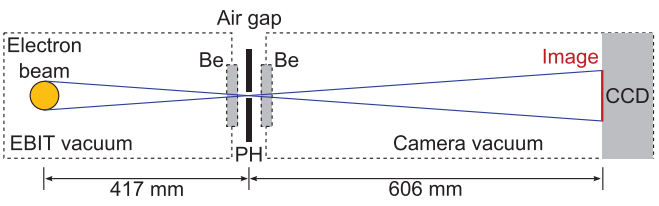

FIG. 2. Schematic view of the pinhole camera set-up (not to scale). The electron beam is imaged on the CCD camera by the slit (PH). This slit is mounted on an xyz-manipulator in an air gap between two Beryllium windows (Be).

The CCD camera is an Andor DO936 which is equipped with a back-illuminated, 2048 $\times$ 2048 pixel CCD chip sensitive to photons in a wide spectral range between the optical regime and 10 keV. The chip has a size of 27.6 mm $\times$ 27.6 mm, giving each pixel an area of (13.5 $\times$ 13.5)μm^2. It is cooled to -50 °C by a Peltier element to reduce the background noise resulting from thermal excitations.

During the X-ray measurements the EBIT is operated with a 4 T magnetic field in the Helmholtz coil region and a 2 T field in the solenoid. An electron beam current of 803 mA with an electron energy of about 15 keV is transported through this field. All trap electrodes are set to the same potential except for the outer barrier electrodes, which are 100 V higher. Including the effect of the electron beam space charge, an axial potential well with a maximum depth of about 250 V in the Helmholtz-region is created on axis of the beam, which is kept constant throughout the measurements. Ions from residual gas such as N, O, C, and Ar as well as heavy ions produced by the cathode (Ba, Os, and W) are accumulated in the trap. Since no "dumping" is applied, i.e., the trap is not emptied periodically, the ion ensemble is assumed to reach thermal equilibrium, with light elements evaporating from the trap and highly charged Ba and W being the main constituents of the ion population. Therefore, the main contributors to the emitted X-rays are expected to be M- and L-shell transitions in Ba and W ions as well as K-shell transitions in Ar ions. The observed X-ray spectrum is cut off on its lower edge at about 2 keV by photon absorption in the Be-windows, while the upper limit of about 10 keV is given by the detection efficiency of the CCD chip.

III. X-RAY IMAGING MEASUREMENT

For the determination of the electron beam radius, a series of measurements was taken for different slit sizes and positions, while keeping all EBIT operation parameters fixed. Due to the low detection solid angle of 1.8 $\times$ 10^{-5}sr for a slit size of 25 μm, an acquisition time of 1800 s was chosen to increase the signal-to-noise ratio. In the first step of data analysis, the X-ray images are corrected for a tilt of the camera and shifted to obtain a horizontal electron beam. This tilt results from a slight misalignment of the CCD pixel rows with respect to the electron beam propagation axis. An example image for a 25 μm slit is shown in Fig. 3(a). For the image profile determination the X-ray images are projected onto the axis perpendicular to the electron beam propagation direction, as depicted in Fig. 3(b). The width of this profile is determined by fitting a Gaussian and taking into account the CCD pixel size of 13.5 μm. The standard deviation σ of the Gaussian is used as a measure of the profile width.

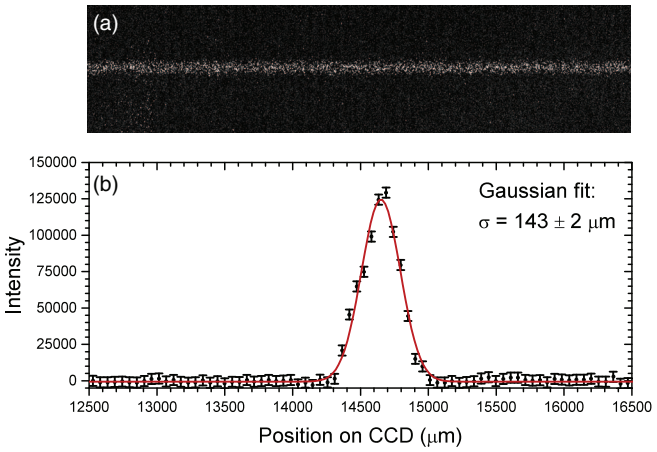

FIG. 3. (a) X-ray image measured with a 25-μm slit width after correction for the camera tilt (see text). (b) Intensity profile obtained by integrating the X-ray counts in image (a) for each row along the electron beam axis. The line represents the result of a Gaussian fit to the data.

Several factors have to be taken into account in the determination of the electron beam radius from the measured width of the image profile. The geometry of the camera set-up provides a magnification factor of $c_M = (1.45 \pm 0.01)$. Furthermore, the observed profile (Fig. 3(b)) is a convolution of the real profile resulting from X-ray emissions of the trapped highly charged ions and the effect of the aperture of the slit. The width of the observed profile is given by

$$\sigma = \sqrt{\sigma_X^2 + \delta_S^2}, \quad (1)$$

with σ_X being the width of the real profile and δ_S the broadening due to the slit aperture. A broadening of the image due to diffraction at the slit is negligible for photon energies above 2 keV. To correct for the effect of the slit aperture, a series of measurements was taken with different slit widths from 25 μm to 500 μm. The result is shown in Fig. 4, where the width σ of the measured profile (corrected for the magnification) is plotted against the slit width. As expected, the slit width has a strong influence on the observed profile if it approaches and exceeds the size of the electron beam. For this reason, a slit width of 25 μm, an order of magnitude smaller than the electron beam radius, is used for the final beam size measurement. By extrapolating the measured dependence to zero width using a third-order polynomial that approximates the convolution of the slit aperture and the real profile, the influence of a finite slit width is determined. A factor of $c_S = (0.97 \pm 0.03)$ is obtained for the correction of the value measured at 25μm.

A series of measurements with the slit at different vertical positions showed a dependence of the observed profile width on this position (see black triangles in Fig. 5(a)). Moreover, when the CCD was exposed to X-ray emissions without the slit in place, the X-ray intensity image was not uniform in the direction perpendicular to the electron beam. Both observations can be explained with the line-of-sight between the camera and the electron beam being obstructed. This obstruction can be caused by a misalignment of the electron beam with respect to the trap structure leading to the line-of-sight being cut by an edge of the 3 mm wide slit aperture on the

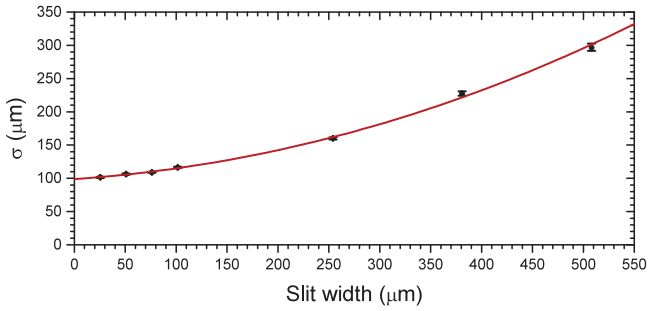

FIG. 4. Measured width of the image profile after Gaussian fit and magnification correction in dependence of the width of the slit.

trap electrode. Furthermore, there are two apertures on the 60 K- and 5 K-shields of the EBIT that could partly block the line-of-sight. As a result, a third correction factor is needed to take into account a possible line-of-sight obstruction.

In order to analyze the influence of this misalignment and hence determine the correction factor, the CCD was exposed to X-rays without the slit assembly. A series of measurements was conducted by moving the electron gun perpendicular to the electron beam axis to slightly move the beam within the trap electrodes while keeping the camera in a fixed position. For each gun position, all counts over the CCD were summed up after subtraction of a background taken without incoming X-rays. The result is shown in Fig. 5(b), where the initial position of the electron gun for the size measurements is marked with a dashed line. A Boltzmann function has been fit to the data points to guide the eye. A plateau of maximum

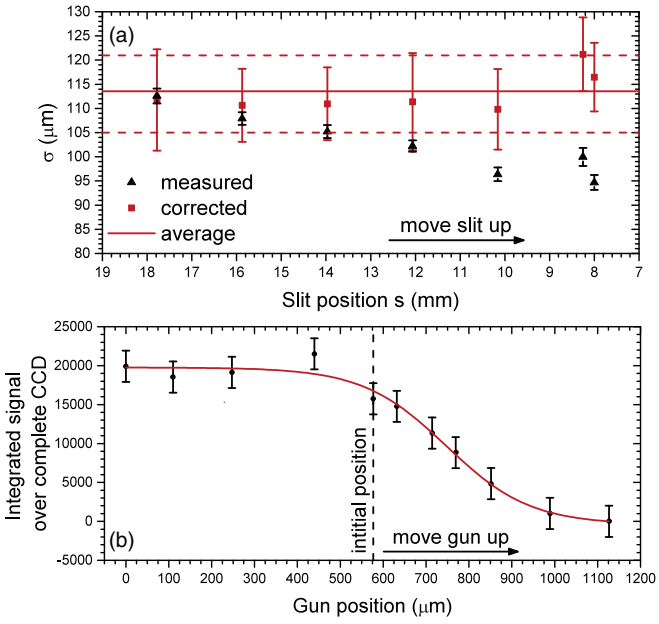

FIG. 5. (a) Standard deviation (σ) of the observed profile as a function of the position of the slit moved in the direction perpendicular to the electron beam axis. Black triangles mark the measured values after correction for the magnification. The measured values after applying all correction factors are shown as red squares. The solid line represents their average and the dashed lines its uncertainty. (b) Integrated X-ray intensity over the entire CCD chip in dependence of the position of the electron gun, taken without the slit. The line represents the fit of a Boltzmann function to the data points, while the dashed line marks the gun position used for the present beam size measurements.

intensity is reached by moving the electron gun down from its initial position by 200 μm or more. Here the X-ray intensity over the CCD is uniform indicating that the line-of-sight is no longer obstructed. These measurements were performed with 100 mA electron beam current since using a current of 800 mA would have led to too high current losses for gun positions away from its initial position. From the 100 mA measurement, a correction factor for the line-of-sight obstruction is obtained that is then applied to the 800 mA measurement with the gun in its initial position.

The correction factor for the obstructed optical path can be calculated from the 100 mA measurements taken with the electron gun in different lateral positions. The factor depends on the region of the CCD where the image occurs. For each slit position s seen in Fig. 5(a), a 200 pixel wide region is selected around the image and the gun position measurement is analyzed for this region. As the intensity on the CCD is proportional to the square of the electron beam radius, a correction factor $c_G(s) = \sqrt{I_0(s)/I_{577}(s)}$ can be calculated for each position from the plateau's maximum intensity I_0 and the intensity I_{577} at the initial gun position of 577 μm. The resulting correction factor ranges between 1% for a slit position of $s = 17.8$ mm and 26% for $s = 8$ mm.

The red solid squares in Fig. 5(a) show the width of the observed profile after all corrections using $\sigma_X = \sigma c_S c_G(s)/c_M$, where σ is the measured value. Averaging over these points, one obtains $\sigma_X = (113 \pm 8)\mu$m for the size of the X-ray image.

A few major sources of systematic errors can effect this measurement. It can be shown from geometric arguments that the images (Fig. 3(a)) observed with the 12.7 mm wide slit aperture represent a 38.9 mm long trap region in axial direction. Within this region, the magnetic field generated by the Helmholtz coils changes by about 2%, which translates to first order into a variation of the electron beam radius by the same amount. This effect cannot be observed in the measurements, since the slit does not image the beam in the axial direction, but contributes to the uncertainty of the results on the level of 2%.

Another source of systematic errors is a possible misalignment of the slit with respect to the electron beam axis. An angle between the slit and beam axis would lead to a broadening of the projected image and to an increase in the number of counts in the center of the image relative to its edges. However, the data do not show significant contributions of these effects. Furthermore, an artificial broadening is minimized in the first step of data analysis which corrects the camera tilt.

Mechanical vibrations can broaden the projected image as well. The camera is not directly attached to the EBIT, but installed on a separate table. To minimize relative vibrations between the camera and the EBIT, this table is firmly attached to the same steel frame the EBIT is mounted on. Furthermore, the camera chamber is not being pumped during the measurements to avoid vibrations caused by the pumps. A measurement of the vibrations of the steel beams and the floor using an accelerometer show a RMS amplitude of 0.8 μm. This value can be used to estimate the vibrations of the CCD camera and has to be included in the result for the image size as a systematic uncertainty.

IV. DETERMINATION OF THE ELECTRON BEAM RADIUS AND CURRENT DENSITY

To extract the radius of the electron beam from the X-ray images, the overlap of the ion cloud with the electron beam has to be considered. Finite-element electron tracking calculations of the ReA-EBIT electron gun in semi-immersed flow mode, performed with the TriComp software, show a nearly flat profile radial current density distribution in the trap.[7,18] Based on these simulations, we assume a cylindrical electron beam with a constant current density $j(r) = I/(\pi r_b^2)$ within the beam radius r_b and the total beam current I. Following the formalism described in Ref. 19, the radial potential $V_e(r)$ of this cylindrical electron beam can be calculated to be

$$V_e(r) = \begin{cases} U_e(r/r_b)^2 & \text{for } r \le r_b \\ U_e(2\ln(r/r_b) + 1) & \text{for } r > r_b \end{cases} \quad (2)$$

satisfying the boundary condition $V_e(0) = 0$ and using $U_e = I/(4\pi\epsilon_0 v)$, where ϵ_0 denotes the vacuum permittivity and v the electron velocity.

The trapped ions of charge state q are expected to be distributed within the radial potential of the electron beam following a Boltzmann distribution:

$$n_i(r) = n_i(0)\exp\left(-qeV(r)/(kT_i)\right), \quad (3)$$

with the ion temperature T_i, Boltzmann's constant k, the ion density on the beam axis $n_i(0)$, and the elementary charge e. The radial ion density distribution $n_i(r)$ can be approximated by a Gaussian profile

$$n_i(r) = N_i/\left(2\pi\sigma_i^2 L\right)\exp\left(-r^2/(2\sigma_i^2)\right), \quad (4)$$

where σ_i is the characteristic ion cloud radius and N_i is the number of ions in the trap of length L. This assumption is justified for an ion cloud within the electron beam, which probes the Gaussian-like shape of the electron beam space charge potential.[14] The electric field of the ion distribution in radial direction can be obtained from Maxwell's equations by integration

$$E_i(r) = \frac{qe}{2\pi\epsilon_0}\frac{1}{r}\int_0^{2\pi}\int_0^r n_i(r')r'dr'd\phi. \quad (5)$$

From this electric field, the radial space charge potential of the ions is calculated as

$$V_i(r) = -\int_0^r E_i(r')dr' = -U_i\left(\frac{r^2}{2\sigma_i^2} - \frac{1}{4}\left(\frac{r^2}{2\sigma_i^2}\right)^2 + \ldots\right), \quad (6)$$

where $U_i = qeN_i/(4\pi\epsilon_0 L)$ and the exponential function is expressed by a series expansion.[19]

The radial potential confining the ions in Eq. (3) is a combination of the electron and ion space charge potentials given in Eq. (2) for $r \le r_b$ and Eq. (6). Neglecting higher order terms of the expansion, the total potential can be expressed as

$$V(r) = V_e(r) + V_i(r) = \left(\frac{U_e}{r_b^2} - \frac{U_i}{2\sigma_i^2}\right)r^2. \quad (7)$$

Comparing the exponents in Eqs. (3) and (4) and combining this with Eq. (7), one obtains

$$\frac{r^2}{2\sigma_i^2} = \frac{qeV(r)}{kT_i} = \frac{qer^2}{kT_i}\left(\frac{U_e}{r_b^2} - \frac{U_i}{2\sigma_i^2}\right), \tag{8}$$

which yields a relation between the characteristic size of the Gaussian ion cloud and the radius of a cylindrical electron beam

$$\frac{\sigma_i}{r_b} = \sqrt{\frac{kT_i + qeU_i}{2qeU_e}}. \tag{9}$$

The photon density in the trap emitted within an acquisition time t_{ac} is given by

$$n_\gamma(r) = \sigma_{ex} n_i(r) j(r) t_{ac}/e, \tag{10}$$

using σ_{ex} as an effective electron impact excitation cross section and assuming an instant photon emission after excitation. For a cylindrical electron beam with a uniform density and a Gaussian ion cloud, the radial photon density $n_\gamma(r)$ has a Gaussian shape as well, thus

$$\begin{aligned} n_\gamma(r) &= n_\gamma(0)/\left(2\pi\sigma_\gamma^2\right) \exp\left(-r^2/\left(2\sigma_\gamma^2\right)\right) \\ &\propto \exp\left(-r^2/\left(2\sigma_i^2\right)\right), \end{aligned} \tag{11}$$

where $n_\gamma(0)$ is the photon density on the electron beam axis and σ_γ is the characteristic size of the photon distribution. Since the current density j is independent of r in this case, the size of the photon distribution equals the size of the ion cloud $\sigma_\gamma = \sigma_i$. Note that this relation changes to $\sigma_\gamma = \sqrt{\sigma_i^2\sigma_e^2/(\sigma_i^2 + \sigma_e^2)}$ for a Gaussian electron current density distribution with a characteristic size σ_e.

The measured image on the CCD is a projection of the photon distribution onto the CCD plane. The characteristic size of the distribution is not changed by this projection, thus $\sigma_\gamma = \sigma_X$. The radius of the cylindrical electron beam can then be extracted from the measured X-ray profile using Eq. (9). For this, values for U_e, U_i, and T_i have to be determined. U_e can be calculated from the known electron beam current I and energy E_e. For $I = 803$ mA and $E_e = 15$ keV, $U_e = (101 \pm 1)V$ is obtained.

U_i is proportional to the total charge of all ions in the trap (charge capacity), which depends on the axial trapping potential. It can be determined using the ion extraction system of the ReA-EBIT:[20] after extraction, the ions are first sent through an electrostatic 90° bender for energy selection and then to a 90° dipole magnet for charge-over-mass separation. By measuring the ion current between the electrostatic bender and the magnet, the total charge of the stored ions can be determined. Typical results yield values for U_i of (7 ± 2)V under operation conditions similar to those of the X-ray imaging measurements.

The average equilibrium temperature of the ions in the trap is the parameter most difficult to determine. A common estimate[21] relates the equilibrium temperature of ions of charge state q with the axial trapping potential V_{ax} as $kT_i \approx (0.1 - 0.4)qeV_{ax}$. The results of ion extraction measurements can be used to get a better estimate of the ion temperature. By determining the width of the ion beam profile behind the energy-dispersive electrostatic 90° bender, the energy spread of the ion beam can be calculated. This spread mainly results from the distribution of the ions in the radial electron beam potential as well as the width of the ion temperature distribution, which both depend on the ion temperature. These measurements yield a temperature per charge of $T_i/q = (39 \pm 3)eV$ or $kT_i \approx (0.15 \pm 0.02))qeV_{ax}$ for the trapping conditions used during the X-ray measurements.[22]

TABLE I. EBIT parameters used for calculating the electron beam radius from Eq. (9) and the final results.

Electron beam current	I (mA)	803(5)
Electron beam energy	E_e (kV)	15.0(1)
Electron beam space charge	U_e (V)	101(1)
Ion cloud space charge	U_i (V)	7(2)
Ion temperature per charge	T_i/q (eV)	39(3)
Cylindrical electron beam radius	r_b (μm)	237(22)
80% electron beam radius	$r_{80\%}$ (μm)	212(19)
Electron beam current density	j (A/cm^2)	454(83)

Using these values and the measured ion cloud size in Eq. (9), the radius for a cylindrical electron beam is calculated to be $r_b = (237 \pm 22)\mu$m. It is more common for comparison to give the 80%-radius, which is defined as the radius of the beam containing 80} of the total beam current I. An 80%-radius of $r_{80\%} = (212 \pm 19)\mu$m is obtained. From the measured radius, a current density of $j = (454 \pm 83)$A/cm^2 between the Helmholtz coils in the 4 T field for 803 mA beam current can be deduced. These results and the values used for the calculation are summarized in Table I.

V. DISCUSSION OF THE RESULTS

Tracking simulations of the electron beam with TriComp including the electron gun parameters and the 4 T field in the Helmholtz region used for the beam size measurement,[7] predict an 80%-radius of $r_{80\%} = 208\,\mu$m. This result agrees with the measured value within the uncertainty. Note that the simulation result also has an uncertainty that is influenced by, e.g., the uncertainty of the magnetic field at the cathode and a possible misalignment of the set-up. The measurement serves as a test for the electron beam trajectory simulations and shows, that the simulations can provide reliable results, which is the basis for a future optimization of the electron gun design.

The charge breeding efficiency of the EBIT for continuous ion injection can be used to estimate the electron beam current density. Experiments with stable ^{39}K ions result in a total charge breeding efficiency of up to 30% (calculated from the ion yield in all charge states compared to the incoming, singly charged ion current) and 6% for $^{39}K^{15+}$ ions.[3] This efficiency can be predicted for a given current density by a simplified model of the ion capture in the EBIT.[7,18] For this purpose, the magnetic field configuration of 4 T in the Helmholtz region and 2 T in the solenoid has to be taken into account. The lower solenoid field leads to an expansion of the electron beam to a higher radius and thus a lower current density. A current density of about 550 A/cm^2 in the 4 T region, leading to an average current density of about 380 A/cm^2 over the full length of the trap, is necessary to reach a capture efficiency of

30% for the experimental conditions. Though not being very accurate, this method indicates that the interpretation of the beam size measurement might underestimate the current density.

The main uncertainty in the interpretation could be the expansion of the ion ensemble. Equation (9) yields $\sigma_i/r_b = 0.47$ for the trapping conditions used, indicating that the ion cloud is smaller in diameter than the electron beam. Thus it is assumed that the observed image represents the ion cloud and not the electron beam. If T_i is actually underestimated, the true electron beam radius would be smaller, thus leading to a higher current density. For a more accurate determination of the ion temperature and the dynamics of the ion cloud, further measurements are necessary. However, an ion temperature high enough to expand the ion cloud far out of the electron beam seems unlikely under the conditions of the measurement. If the ion cloud was much larger in diameter than the electron beam, a Gaussian electron beam density would have to be assumed given the observed Gaussian profile, which would then change the interpretation of the observations. This scenario requires replacing $r_b/\sqrt{2}$ in Eq. (9) by the characteristic size of the Gaussian beam, which would result in a higher electron beam radius.

Furthermore, neglecting the fourth-order term in Eq. (6) can have an influence on the resulting cylindrical electron beam radius. The r^4-term is estimated to change the ion space charge potential at $r = \sigma_i$ by about 12%. This increases the total potential $V(\sigma_i)$ from Eq. (7) by about 2%. To quantify the effect of this increase on the electron beam radius, the Gaussian function in Eq. (3) was directly fit to the intensity profile (Fig. 3(b)) for one slit position of Fig. 5(a), including all correction factors and the r^4-term of the ion space charge potential. The resulting electron beam size deviates from the result obtained without the higher-order term by less than 4% and neglecting it is a small effect compared to the uncertainty of the final result.

VI. CONCLUSION

X-ray imaging measurements using a pinhole camera reveal an electron beam radius of $r_{80\%} = (212 \pm 19)\mu$m in the 4T magnetic field region of the ReA-EBIT. This radius is a basic characteristic of the device and defines its electron beam current density. It leads to a current density of $j = (454 \pm 83)$A/cm^2 assuming a cylindrical electron beam. The current density is one of the main factors determining the charge breeding efficiency and thus the performance of the EBIT. The radius agrees with simulations of the electron gun in the semi-immersed cathode configuration.[7] The current density is also in satisfactory agreement with recent charge breeding efficiency measurements.[3]

One of the goals for future developments of the ReA-EBIT is an increase of the electron beam current density. First steps currently taken are an increase of the magnetic field to a 4T-4T configuration and of the electron beam current to 1.4 A. This will result in a predicted total efficiency of about 50% for continuous ion injection. Furthermore, a re-design of the electron gun for a stronger electron beam compression while maintaining a high total current can yield even higher current densities.

ACKNOWLEDGMENTS

The authors thank C. Rau for his contributions to the mechanical set-up. This work was supported by Michigan State University (MSU) and the National Science Foundation (NSF) under Contract No. PHY-1102511.

[1] D. Leitner, D. Alt, T. M. Baumann, C. Benatti, K. Cooper, B. Durickovich, K. Kittimanapun, S. Krause, A. Lapierre, L. Ling-Ying, F. Montes, D. Morrissey, S. Nash, R. Rencsok, A. J. Rodriguez, C. Sumithrarachchi, S. Schwarz, M. Steiner, M. Syphers, S. Williams, W. Wittmer, and X. Wu, in *Proceedings of PAC2013* (JACoW (Joint Accelerator Conferences Website), Pasadena, CA, 2013), pp. 1458–1462.
[2] G. Bollen, C. Campbell, S. Chouhan, C. Guénaut, D. Lawton, F. Marti, D. J. Morrissey, J. Ottarson, G. Pang, S. Schwarz, A. F. Zeller, and P. Zavodszky, Nucl. Instrum. Meth. B **266**, 4442 (2008).
[3] A. Lapierre, S. Schwarz, T. M. Baumann, K. Cooper, K. Kittimanapun, A. J. Rodriguez, C. Sumithrarachchi, S. J. Williams, W. Wittmer, D. Leitner, and G. Bollen, Rev. Sci. Instrum. **85**, 02B701 (2014).
[4] F. Herfurth, K. Blaum, S. Eliseev, O. Kester, H.-J. Kluge, S. Koszudowski, C. Kozhuharov, G. Maero, D. Neidherr, W. Quint, S. Schwarz, S. Stahl, and G. Vorobjev, Hyperfine Interact. **173**, 93 (2006).
[5] F. Wenander, P. Delahaye, R. Scrivens, R. Savreux, and REX-Isolde-Collaboration, Rev. Sci. Instrum. **77**, 03B104 (2006).
[6] M. Leitner, J. Bierwagen, J. Binkowski, S. Bricker, C. Compton, J. Crisp, L. Dubbs, K. Elliot, A. Facco, A. Fila, R. Fontus, A. Fox, P. Gibson, P. Guetschow, L. Harle, M. Hodek, J. Holzbauer, M. Johnson, S. Jones, T. Kole, B. Lang, D. Leitner, I. Malloch, F. Marti, D. Miller, S. Miller, T. Nellis, D. Norton, R. Oweiss, J. Popielarski, L. Popielarski, X. Rao, G. Velianoff, N. Verhanovitz, J. Wei, J. Weisend, M. Williams, K. Witgen, J. Wlodarczak, Y. Xu, and Y. Zhang, in *Proceedings of SRF2011* (JACoW (Joint Accelerator Conferences Website), Chicago, IL, 2011), pp. 56–64.
[7] S. Schwarz, T. M. Baumann, K. Kittimanapun, A. Lapierre, and A. Snyder, Rev. Sci. Instrum. **85**, 02B705 (2014).
[8] R. Becker and O. Kester, Rev. Sci. Instrum. **83**, 02A506 (2012).
[9] D. A. Knapp, R. E. Marrs, S. R. Elliott, E. W. Magee, and R. Zasadzinski, Nucl. Instrum. Meth. A **334**, 305 (1993).
[10] S. B. Utter, P. Beiersdorfer, J. R. Crespo López-Urrutia, and K. Widmann, Nucl. Instrum. Meth. A **428**, 276 (1999).
[11] N. Nakamura, A. Ya. Faenov, T. A. Pikuz, E. Nojikawa, H. Shiraishi, F. J. Currell, and S. Ohtani, Rev. Sci. Instrum. **70**, 1658 (1999).
[12] A. Silze, G. Zschornack, V. P. Ovsyannikov, and F. Ullmann, Rev. Sci. Instrum. **79**, 083302 (2008).
[13] Y. Yang, L. Di, F. Yun-Qing, Y. Ke, C. Wei-Dong, X. Jun, G. Zhi-Xian, R. Hutton, and Z. Ya-Ming, Chin. Phys. B **20**, 080701 (2011).
[14] J. V. Porto, I. Kink, and J. D. Gillaspy, Rev. Sci. Instrum. **71**, 3050 (2000).
[15] J. R. Crespo López-Urrutia, P. Beiersdorfer, K. Widmann, and V. Decaux, Can. J. Phys. **80**, 1687 (2002).
[16] V. Mäckel, R. Klawitter, G. Brenner, J. R. Crespo López-Urrutia, and J. Ullrich, Phys. Rev. Lett. **107**, 143002 (2011).
[17] A. Lapierre, S. Schwarz, K. Kittimanapun, J. Fogleman, S. Krause, S. Nash, R. Rencsok, L. Tobos, G. Perdikakis, M. Portillo, J. A. Rodriguez, W. Wittmer, X. Wu, G. Bollen, D. Leitner, and M. Syphers, AIP Conf. Proc. **1525**, 497 (2013).
[18] K. Kittimanapun, T. M. Baumann, A. Lapierre, S. Schwarz, and G. Bollen, "Acceptance Calculation for Continuous Ion Beam Injection into the Electron Beam Ion Trap Charge Breeder of the ReA Post-Accelerator," (unpublished).
[19] R. Marrs, Nucl. Instrum. Meth. B **149**, 182 (1999).
[20] M. Portillo, G. Bollen, S. Chouhan, O. Kester, G. Machicoane, J. Ottarson, S. Schwarz, and A. Zeller, in *Proceedings of PAC2009* (JACoW (Joint Accelerator Conferences Website), Vancouver, BC, Canada, 2009), pp. 4341–4343.
[21] F. J. Currell, in *The Physics of Multiply and Highly Charged Ions*, Volume 1 (Dordrecht, The Netherlands, 2003).
[22] T. M. Baumann, A. Lapierre, G. Bollen, K. Kittimanapun, S. Schwarz, and C. Sumithrarachchi, "Energy Spread and Time Structure of Ion Beams extracted from the ReA-EBIT Rare Isotope Charge Breeder," AIP Conf. Proc. (unpublished).